Synchrophasor Network-Based Detection and Classification of Power System Events: A Singular Value Decomposition Approach

Reza Pourramezan, Houshang Karimi, and Jean Mahseredjian

***Abstract*—Timely detection and classification of power system events are essential for situation awareness and reliable electricity grid operation. It is also a crucial step with regard to synchrophasor network data management and archiving. In this paper, an event detection and classification method based on the singular value decomposition (SVD) of synchrophasor data is proposed. The detection algorithm exploits the low-dimensionality characteristics of synchrophasor data and identifies the changes in the dimensionality of a sliding data matrix. The SVD-based method assigns several detection flags indicating events and outliers in voltage magnitude, phase angle and frequency data. The proposed classification algorithm comprises a decision tree employing detection flags and singular values to classify events into several categories, e.g., fault, voltage magnitude and phase angle events, and generation-load mismatch events. Moreover, the proposed algorithm identifies whether events are spatially correlated. Field synchrophasor data collected from a smart grid are used to evaluate the performance of the proposed method. The numerical results show that the proposed method can successfully detect and classify different types of events even in the presence of measurement uncertainty.**

***Keywords*—Event detection, phasor measurement unit (PMU), singular value decomposition, synchrophasor.**

I. Introduction

SYNCHROPHASOR data produced by PMUs are key measurements used in the monitoring, protection, and control of the modern electric grid by providing accurate and timestamped snapshots of the power system [1]. In transmission and distribution systems, events such as oscillations, line tripping, faults, and islanding can lead to grid instability and power outages. The post-event analysis of synchrophasor data has shown that offline techniques can help reconstruct different scenarios and identify the root cause of the events [2]. Given the sheer amount of synchrophasor data in PMU networks and the limited archive space, it is crucial to detect and classify events, discard older irrelevant measurements, and only compress and archive measurements required for post-event analysis. In real-time, the classification of these events and decision-making is even more complex.

R. Pourramezan is with New York Power Authority, NY 10601 USA (e-mail of the corresponding author: reza.pourramezan@nypa.gov). H. Karimi is with the Department of Electrical Engineering & Computer Science, York University, Toronto, ON M3J 1P3 Canada (e-mail: hkarimi6@yorku.ca). J. Mahseredjian is with the Department of Electrical Engineering, Polytechnique Montreal, Montreal, QC H3T 1J4 Canada (e-mail: jean.mahseredjian@polymtl.ca).

Paper submitted to the International Conference on Power Systems Transients (IPST2023) in Thessaloniki, Greece, June 12-15, 2023.

There are various data-driven synchrophasor-based event detection, spatial localization, and characterization methods that use isolation forest, dynamic programming, clustering technique, Prony analysis, and decision tree [3]–[7]. Most of the existing methods do not consider the stochastic, dynamic, and nonlinear characteristics of power systems and rely on data labelling and feature selection. Particularly, the low-rank characteristics and spatial-temporal (spatiotemporal) correlations of PMU data are not leveraged.

A synchrophasor matrix of several PMUs data is low-rank due to the spatiotemporal similarities. Similar to principal component analysis (PCA), singular value decomposition (SVD) of the synchrophasor data matrix decomposes it into several singular modes. The first few singular modes have the most significant contribution to the original data. However, the higher-dimension modes usually contain PMU measurement error and noise. When an event or outlier happens, the spatiotemporal correlation changes and the required number of singular modes to accurately reconstruct the data (the dimensionality of the data matrix) increases. Several PCA/SVD-based methods leveraging the low-rank characteristics have been proposed to address synchrophasor data problems such as missing data recovery [8], data compression [9]–[11], and event/outlier detection [12]–[14].

A PCA-based method for online characterization of outliers in synchrophasor data is proposed in [12]. The dynamic responses of a system under nominal and off-nominal (e.g., faulted) conditions are analyzed and a bound on the change in the norm of the principal component (PC) scores is presented. It is shown that in the presence of bad data outliers, these bounds for higher dimensional PC scores will be significantly larger compared to lower dimensions. However, real-time detection and event classification are not addressed.

PCA is used in [13] to analyze dimensionality reduction. When an event occurs, an alert from the early event detection algorithm is issued if the proposed event indicator becomes very large due to the change in the core subspaces of the PMU data. However, small events may not trigger the event indicator, event classification is not proposed, and an adaptive training stage is required to extract the key features of the high-dimensional PMU data.

In [14], the low-dimensional subspace spanned by the dominant singular vectors of the data matrix is used to characterize an event and a dictionary of subspaces should be established using offline training data. The dictionary is used to match the online events with the most similar event

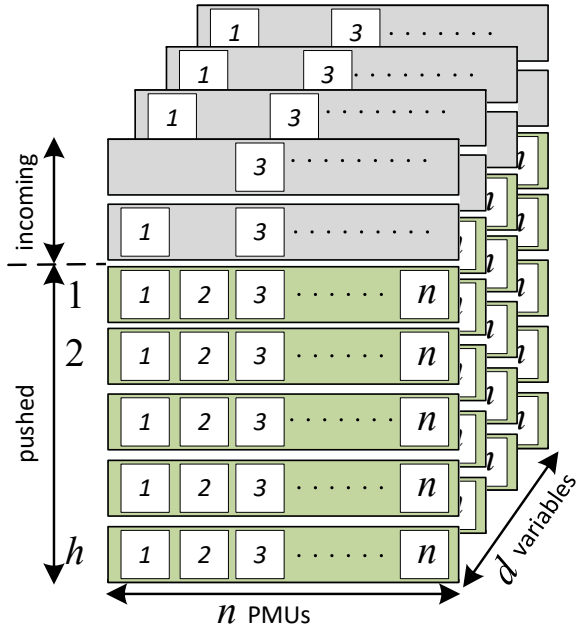

Fig. 1. Block diagram of a typical PDC buffer.

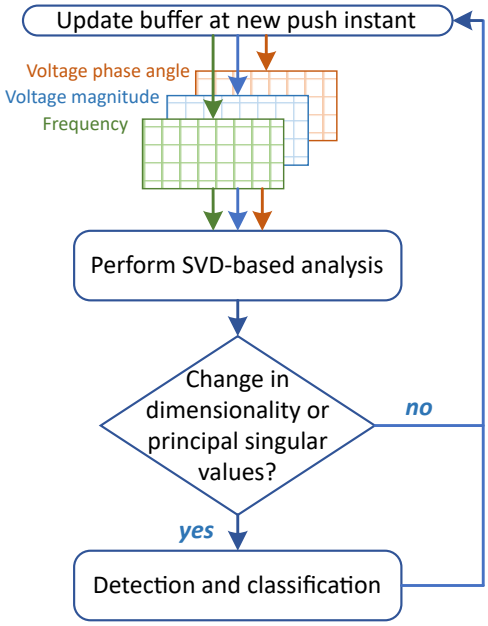

Fig. 2. Simplified flowchart of the proposed method

in the dictionary through subspace comparison. However, establishing an efficient offline dictionary requires a massive amount of training event data which is a big challenge in real power systems. Moreover, the dominant singular vector selection is performed using two experimental thresholds that can introduce over/under-estimation of the subspace rank. The choice of singular value thresholding criteria is a common challenge in all PCA/SVD-based methods applied to synchrophasor data and should be addressed [10]–[16].

In this paper, we propose an SVD-based method to detect and classify power system events using real-time synchrophasor data collected by a phasor data concentrator (PDC) from different locations. The proposed method performs dimensionality analysis on a real-time sliding window to detect events and classify them based on the changes in the dimensionality and singular values of data matrices including voltage magnitude, phase angle, and frequency data. Compared to existing PCA/SVD-methods, the main contributions of this paper are threefold:

1) The proposed singular value thresholding criterion is not experimental. Instead, we use PMU accuracy information provided by the manufacturer to set the thresholds and hence guarantee both reliability and security of low-rank subspace estimation.
2) The proposed data-driven method does not require training event data which is challenging to obtain from real systems and uses online voltage magnitude, phase angle, and frequency SVD results for direct classification.
3) The proposed algorithm has a low computational burden and is capable of detecting events at an earlier stage compared to training-based classifiers and raw PMU data monitoring approaches.

The rest of the paper is organized as follows. Section II presents the outline of the proposed detection and classification method. Section III describes the proposed core SVD-based dimensionality approximation and the respective singular value thresholding method. The proposed detection and decision tree classifier algorithms are detailed in Section IV. The numerical results using field synchrophasor data of a real microgrid are presented in Section V. Finally, Section VI includes the summary and conclusions.

II. Outline of the Proposed Method

Figure 1 shows the structure of a PDC with d circular buffers each for a variable such as frequency, magnitude, and phase angle of voltage and current signals [17]. The buffers have n columns each dedicated to a PMU and h completed (pushed) rows. With a PDC refreshing rate of F_s frames per second (fps), the rows represent intervals of $1/F_s$ second. We employ the buffer history (bottom part) with the duration of h/F_s second and construct the general data matrix $\mathbf{Y}$ as

$$\mathbf{Y} = \begin{bmatrix} \mathbf{y_1} & \mathbf{y_2} & \cdots & \mathbf{y_n} \end{bmatrix} \tag{1}$$

where $\mathbf{y_i}$ with $i = [1, \cdots, n]$ are temporal data vectors with the length of h. The observed data matrix $\mathbf{Y}$ includes the ground-truth data $\mathbf{X}$ and the measurement error $\mathbf{E}$ such that

$$\mathbf{Y} = \mathbf{X} + \mathbf{E}\,. \tag{2}$$

However, matrices $\mathbf{X}$ and $\mathbf{E}$ are not observed and cannot be analytically determined since $\mathbf{E}$ is a random process. The elements of each row of $\mathbf{Y}$ are spatially correlated since they represent the measurements reported from PMUs at a given timestamp. On the other hand, the elements of each column of $\mathbf{Y}$ are temporally correlated. Due to the spatiotemporal correlations in synchrophasor data, $\mathbf{Y}$ exhibits low-rank characteristics. Therefore, we can use SVD to estimate the dimensionality of $\mathbf{Y}$. As soon as the first instant of an event or outlier data enters the first row of the sliding matrix $\mathbf{Y}$, the spatiotemporal correlations decrease and the dimensionality of the data increases. The main idea is to

continuously assess the dimensionality of $\mathbf{Y}$ in real-time and determine whether any changes occur in the spatiotemporal correlations or in the magnitude of SVD modes.

Figure 2 describes the outline of the proposed event detection method. At each PDC push instant, the buffers containing the measured voltage magnitudes, phase angles, and frequencies are updated and converted to data matrices $\mathbf{Y}$ with the structure given in (1). SVD is performed for each data matrix and used to determine the dimensionality of each variable. If the dimensionality of any of data matrices is increased from its nominal value or any of the primary singular values is deviated significantly from its average value, an event is declared. Subsequently, the results of SVD are sent to detection and classification algorithms. The following sections describe the synchrophasor data dimensionality approximation, event detection, and classification methods.

III. SVD-BASED DIMENSIONALITY APPROXIMATION

Given $m = min(h, n)$, the reduced SVD of $\mathbf{Y}$ becomes

$$\mathbf{Y} = \sum_{r=1}^{m} \sigma_r \mathbf{u}_r \mathbf{v}_r^T \tag{3}$$

where $\{\mathbf{v}_1, \mathbf{v}_2, \cdots, \mathbf{v}_m\}$ and $\{\mathbf{u}_1, \mathbf{u}_2, \cdots, \mathbf{u}_m\}$ are the right and left singular vectors, respectively, and $\sigma_1, \sigma_2, \cdots, \sigma_m$ are the corresponding singular values. Singular vectors $\mathbf{u}_r$ and $\mathbf{v}_r$ are the temporal and spatial eigenfunctions of $\mathbf{Y}$, respectively, and are normalized so that

$$\sqrt{\sum\nolimits_{i=1}^{h} \mathbf{u}_r(i)^2} = 1 \tag{4}$$

$$\sqrt{\sum\nolimits_{j=1}^{n} \mathbf{v}_r(j)^2} = 1 \tag{5}$$

Thus, the SVD results in m modes, each consisting of a temporal mode shape ($\mathbf{u}_r$), a spatial mode shape ($\mathbf{v}_r$), and a mode magnitude (σ_r). The contribution of the r^{th} SVD mode to $\mathbf{Y}$ is given, according to [18,19], as

$$\mathbf{Y}_r = \sigma_r \mathbf{u}_r \mathbf{v}_r^T \tag{6}$$

Due to the spatiotemporal correlations in synchrophasor data, the first few modes capture the primary dynamics of the data matrix, and measurement errors and small perturbations are reflected in the higher dimension modes. Therefore, the dimensionality of $\mathbf{Y}$ is determined by the number of the first ρ modes, and the best rank-ρ approximation to $\mathbf{Y}$ is constructed as given in [20]:

$$\mathbf{Y}_\rho = \sum_{r=1}^{\rho} \mathbf{u}_r \sigma_r \mathbf{v}_r^T \tag{7}$$

According to [19], the threshold criterion to find ρ should determine whether the magnitude of a mode is larger than the measurement error which is represented as noise matrix in (2). In words, only the modes with signal-to-noise ratio (SNR) greater than unity are validated and the rest are rejected. As shown in [9], the SNR of the r^{th} SVD can be calculated as

$$\text{SNR}_r = \left(\frac{\mathbf{Y}_{r\,RMS}}{\mathbf{E}_{RMS}} \right)^2 \tag{8}$$

where $\mathbf{Y}_{r\,RMS}$ and $\mathbf{E}_{RMS}$ are the RMS amplitudes of $\mathbf{Y}_r$ and $\mathbf{E}$, respectively. Therefore, the condition to validate the r^{th} mode with SNR greater than unity is $\mathbf{Y}_{r\,RMS} > \mathbf{E}_{RMS}$. In order to determine ρ, we should calculate $\mathbf{Y}_{r\,RMS}$ and a bound on the RMS error $\mathbf{E}_{RMS}$ [19]. Calculating the RMS using (6) yields

$$\begin{aligned} \mathbf{Y}_{r\,RMS} &= \sqrt{\frac{1}{hn} \sum\nolimits_{i=1}^{h} \sum\nolimits_{j=1}^{n} \mathbf{Y}_r(i,j)^2} \\ &= \frac{\sigma_r}{\sqrt{hn}} \sqrt{\sum\nolimits_{i=1}^{h} \mathbf{u}_r(i)^2} \sqrt{\sum\nolimits_{j=1}^{n} \mathbf{v}_r(j)^2} \\ &= \frac{\sigma_r}{\sqrt{hn}} \,. \end{aligned} \tag{9}$$

Moreover, as shown in [9], it can be assumed that the random process $\mathbf{E}$ has an upper bound ϵ such that

$$\mathbf{E}_{RMS} \leq \epsilon. \tag{10}$$

Therefore, the condition to validate the r^{th} mode becomes $\sigma_r / \sqrt{hn} > \epsilon$. Thus, we define a threshold $\hat{\sigma}$ such that

$$\hat{\sigma} \triangleq \epsilon \sqrt{hn} \tag{11}$$

which gives the singular value thresholding criterion $\sigma_r > \hat{\sigma}$. Thus, the reduced dimensionality of $\mathbf{Y}$ is determined as the total number of SVD modes that satisfy the condition $\sigma_r > \hat{\sigma}$:

$$\rho = \sum_{r=1}^{m} \begin{cases} 1, & \text{if } \sigma_r > \hat{\sigma} \\ 0, & \text{otherwise.} \end{cases} \tag{12}$$

In order to determine the upper bound ϵ on $\mathbf{E}$, we use the accuracy metrics provided by PMU manufacturers. The PMU measurement accuracy is usually given by metrics such as magnitude error (ME), angle error (AE), and frequency error (FE) that represent the maximum error of different measurement types. Therefore, to calculate (11) for each type of data matrix, we use the corresponding metric, i.e., ME, AE, or FE as the upper bound ϵ.

IV. SVD-BASED EVENT DETECTION AND CLASSIFICATION

In this section, the proposed SVD-based event detection and classification methods are described.

A. SVD-based Detection

Algorithm 1 describes the proposed SVD-based event detection method that is executed at each PDC push instant. Data matrices $\mathbf{Y}_i$ including the frequency, voltage magnitude, and voltage phase angle of different phases are updated and any missing entries are recovered using methods such as [8]. PMU acuuracy information including FE, ME, and AE are used as ϵ_i with $i = \{1, \cdots, d\}$.

A detection flag ϕ_i is assigned to each data variable which is set to 0 for normal operating conditions and 1 when an event is detected. During initialization (Line 1), the algorithm does not evaluate the $\mathbf{Y}_i$ until the buffer is full after h instants.

After initialization, Subroutine 1 is executed for all $\mathbf{Y}_i$ to determine flags ϕ_i. The reduced SVD is calculated in Line 3, and the dimensionality of $\mathbf{Y}_i$ is approximated in Line 4. The flag ϕ_i is set using Line 5 to Line 9. The flag is set to 0 if there

Algorithm 1 SVD-based event detection

Inputs: Matrices $\mathbf{Y}_i$ and PMU accuracy ϵ_i for $i = \{1, \cdots, d\}$ as data type, e.g., magnitude, phase angle, and frequency.
Outputs: Detection flags ϕ_i, and $\bar{\phi}_i$

1: **Initialisation**: Wait for h instants until buffer is full

2: **for** $i \leftarrow 1, \cdots, d$ **do**

Subroutine 1: SVD-based analysis

3: Perform reduced SVD: $\mathbf{Y}_i = \sum_{r=1}^{m} \sigma_{ir} \mathbf{u}_{ir} \mathbf{v}_{ir}^T$

4: Approximate dimensionality using (12):

$$\rho_i = \sum_{r=1}^{m} \begin{cases} 1, & \text{if } \sigma_{ir} > \epsilon_i \sqrt{hn} \text{ using (11)} \\ 0, & \text{otherwise.} \end{cases}$$

5: **if** $\rho_i > \rho_{ni}$ **then** ▷ Check dimensionality change

6: $\phi_i = 1$ ▷ Dimensionality has changed

7: **else**

8: $\phi_i = 0$ ▷ No change in dimensionality

9: **end if**

10: Update the moving average of the first singular value: $\bar{\sigma}_{i1} = \sum_{j=t-\frac{L-1}{F_s}}^{t} \sigma_{i1}(j)$

11: **if** $|\sigma_{i1} - \bar{\sigma}_{i1}|/\bar{\sigma}_{i1} > \alpha$ **then**

12: $\bar{\phi}_i = 1$ ▷ Singular value change flag

13: **else**

14: $\bar{\phi}_i = 0$ ▷ No change in singular value

15: **end if**

16: **end for**

Algorithm 2 Event classification

Inputs: Detection flags ϕ_i & $\bar{\phi}_i$ and singular values σ_{i1} & σ_{i2} determined by Algorithm 1 where indices $i = \{1, 2, 3\}$ correspond to voltage magnitude (vm), voltage phase angle (pa), and frequency (f), respectively.

1: **if** any $\phi_i = 1$ OR $\bar{\phi}_i = 1$ **then** ▷ Event detected

2: **if** all ϕ_{vm}, ϕ_{pa} & ϕ_f are equal to **1 then**

3: Significant decrease in all σ_{i1} & increase in σ_{i2}: Fault detected.

4: **else if** $\phi_{vm} = 1$ **then**

5: Spatially uncorrelated voltage magnitude event.

6: **if** Significant deviation in σ_{vm1} & σ_{vm2} **then**

7: Step changes downstream of transformer: OLTC operation

8: **end if**

9: **if** Deviation in σ_{vm1}, σ_{vm2} & σ_{pa2} **then**

10: Voltage sag, impulse

11: **end if**

12: **else if** $\phi_{pa} = 1$ **then**

13: Spatially uncorrelated voltage phase angle event with significant deviation in σ_{pa2}: Impulse due to

14: temporary imbalance in load/generation locally.

15: **else if** $\phi_f = 1$ **then**

16: Deviation in σ_{f1} & σ_{f2}: Islanding event.

17: **else if** $\bar{\phi}_{vm} = 1$ **then**

18: Spatially correlated magnitude event with deviation in σ_{vm1}: load switching, step changes

19: **else if** $\bar{\phi}_{pa} = 1$ **then**

20: Spatially correlated voltage phase angle event with deviation in σ_{pa1}: transients, phase angle jump

21: **else if** $\bar{\phi}_f = 1$ **then**

22: Spatially correlated frequency event with deviation in σ_{f1}: Oscillations, sudden load/gen. imbalance

23: **end if**

24: **else**

25: No event detected

26: **end if**

is no change and is set to 1 if it increases from the nominal dimensionality ρ_{ni} determined using some training data.

Spatially correlated events with small magnitudes, do not diminish the low-rank properties of the data matrix. Therefore, events such as a small step in voltage magnitude of all busses do not trigger the dimensionality change detection flag ϕ_i. However, such variation in the magnitude of all PMU measurements changes the value of the first singular value σ_1 which represents the primary dynamics of the data. Hence, we propose an additional detection flag $\bar{\phi}_i$ based on the variation of σ_{i1}. The moving average of the first singular value $\bar{\sigma}_{i1}$ during the last L instants is updated in Line 10. If the instantaneous σ_{i1} deviates from $\bar{\sigma}_{i1}$ such that $|\sigma_{i1} - \bar{\sigma}_{i1}|/\bar{\sigma}_{i1} > \alpha$, then $\bar{\phi}_i$ is set to 1. Here, $\alpha > 0$ is the threshold coefficient. The procedure to determine $\bar{\phi}_i$ is given in Line 11 to Line 15.

B. Event classification

Algorithm 2 summarizes the proposed event classification approach customized for the distribution system under study. The algorithm is executed at each timestamp with intervals of $1/F_s$ seconds. The inputs to Algorithm 2 are the detection flags ϕ_i and $\bar{\phi}_i$ and singular values σ_{i1} and σ_{i2} received from Algorithm 1. Indices $i = \{1, 2, 3\}$ correspond to voltage magnitude (vm), voltage phase angle (pa), and frequency (f), respectively. Therefore, flags for voltage magnitude, phase angle, and frequency are denoted by ϕ_{vm}, ϕ_{pa}, and ϕ_f, respectively. We utilize the fact that the amplitude of the first singular value σ_1 corresponds to the signals' magnitude, and the second singular value σ_2 deviates due to impulses and outliers [12].

An event is declared if any detection flag is set to 1 (Line 1). Faults significantly affect all types of measurements in a short time interval. Therefore, a fault is detected if all flags ϕ_f, ϕ_{vm}, and ϕ_{pa} are set to 1 (Line 2). During a fault, there will be a significant deviation in both σ_{i1} and σ_{i2}.

Events that are not spatially correlated result in dimensionality change and trigger one of the ϕ_{vm}, ϕ_{pa}, or ϕ_f flags (Lines 4 to 15). When OLTC operates, the voltage magnitudes of buses downstream of OLTC change while those upstream remain relatively unchanged. This will cause both σ_{vm1} (step change in overall magnitude) and σ_{vm2} (dimensionality increase) to deviate from their average values. This is used to classify OLTC operation in Line 6. Impulse magnitude events (voltage sag) have a short duration and are thought to happen due to temporary imbalances in load/generation locally, inrush current, or self-clearing

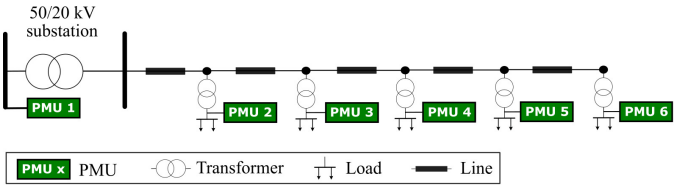

Fig. 3. Single-line diagram of EPFL campus smart grid.

TABLE I
PMU ACCURACY ϵ AND CORRESPONDING SINGULAR VALUE THRESHOLDS $\hat{\sigma}$ FOR DIFFERENT VARIABLES.

Parameter	PMU Accuracy ϵ	Threshold $\hat{\sigma}$
Magnitude	ME: 3.56×10^{-4}	0.0107
Phase Angle	AE: 4.19×10^{-4}	0.0126
Frequency	FE: 3.88×10^{-4}	0.0067

faults upstream. Since small voltage sags happen shortly, their impact on the overall magnitude of the moving window $\mathbf{Y_{vm}}$ is small and does not affect σ_{vm1} for long. However, voltage sag will be reflected in the significant deviation of the second singular values σ_{vm2} and σ_{pa2}. Voltage sag events and impulses, in general, are classified in Line 9 and Line 12. During an islanding event, the frequency of the islanded section deviates from that of the rest of the grid. Therefore, while both σ_{f1} and σ_{f2} deviate, ϕ_f is triggered (Line 15).

Spatially correlated events are detected when one of the $\bar{\phi}_{vm}$, $\bar{\phi}_{pa}$, or $\bar{\phi}_f$ flags is triggered (Lines 17 to 21). Since the amplitudes of all the signals change to a new value, the first singular value representing the primary dynamics of the system will be affected more than other singular values. Step changes in all bus voltages are due to load switching and are detected in Line 17 when $\bar{\phi}_{vm}$ is triggered and only σ_{vm1} deviates due to overall magnitude change with no dimensionality change. Increase and decrease in σ_{vm1} signifies load switch-off (voltage step up) and load switch-on (voltage step down), respectively. Correlated phase angle events such as phase angle jump are declared when $\bar{\phi}_{pa}$ is triggered and σ_{vm1} deviates (Line 19). Oscillations due to generation-load mismatch events cause a significant rise or drop in all frequencies reported from different buses, and are declared when $\bar{\phi}_f$ is triggered (Line 21).

V. Numerical Results

The performance of the proposed detection and classification method is evaluated using field synchrophasor data. Figure 3 shows the single-line diagram of the smart grid of the École Polytechnique Fédérale de Lausanne (EPFL) campus comprising a real-time PMU-based monitoring system. This active smart grid includes photovoltaic panels and combined heat and power units. The nominal frequency of the power system is $f_n = 50$ Hz. The six class-P PMUs employ the enhanced-Interpolated Discrete Fourier Transform synchrophasor approximation method [21]. PMU data are collected and aggregated by a low-latency PDC with the refreshing rate of 50 fps. Detailed information on the PMUs and the smart grid technology can be found in [21]–[23]. The

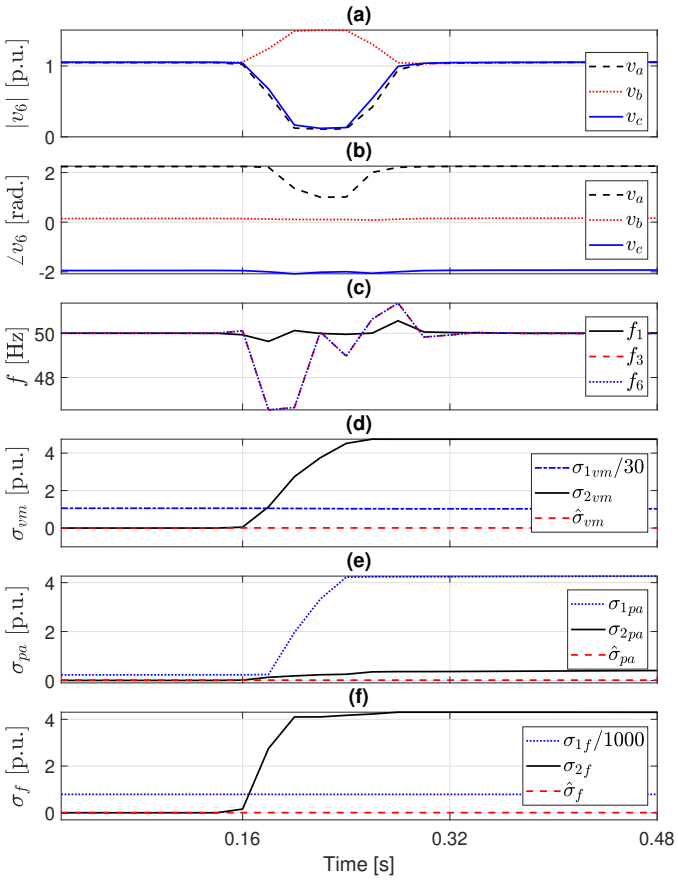

Fig. 4. Detection and classification of a double line to ground fault. (a) voltage magnitude, (b) phase angle, (c) frequency, (d) σ_{vm}, (e) σ_{pa}, and (f) σ_f.

field synchrophasor data used in this paper are made available via the web interface https://smartgrid.epfl.ch/.

The length of data matrices is set to $h = 50$ equal to one second of synchrophasor data. The frequency data matrix $\mathbf{Y}_f$ has 6 columns each assigned to a PMU. The three-phase voltage magnitude and phase angle data of the 6 PMUs are included in $\mathbf{Y}_{vm}$ and $\mathbf{Y}_{pa}$, respectively. Therefore the number of columns in $\mathbf{Y}_{vm}$ and $\mathbf{Y}_{pa}$ is $n = 18$. The accuracy information, i.e., ME, AE and FE, of PMUs used in EPFL are given in [23]. Table I shows these 3 PMU accuracy data used as ϵ_i with $i = [1, 2, 3]$, in (11) to calculate the thresholds $\hat{\sigma}_i$. Moreover, the threshold coefficient $\alpha = 1\%$ is set to determine the detection flags $\bar{\phi}_i$ (see Line 11 of Algorithm 1).

Figures 4(a), (b) and (c) show the voltage magnitude, phase angle, and frequency reported by PMU-6 during a self-clearing double-line to ground fault near the end of the line. It can be seen that the fault temporarily affects all the system variables. Therefore, as shown in Figures 4(d), (e), and (f), the second singular values σ_{2i} of the voltage magnitude, phase angle, and frequency data matrices increase above the respective thresholds $\hat{\sigma}_i$. Therefore, the dimensionality of all variables increase from 1 to 2, and the respective flags ϕ_{vm}, ϕ_{pa}, ϕ_f are triggered. Algorithm 2 correctly classifies this event using the condition given in Line 2.

Figures 5(a), (b), and (c) show three voltage sag events affecting voltage magnitude, phase angle, and frequency of all the nodes in the power system. These voltage sag events with

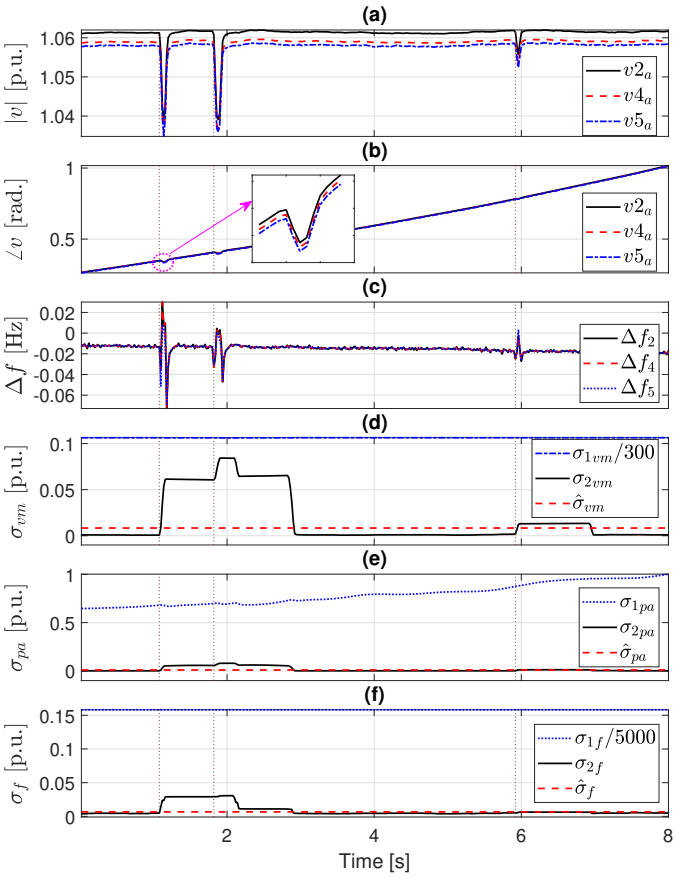

Fig. 5. Detection and classification of multiple voltage sag events caused by faults in upstream power system. (a) voltage magnitude, (b) phase angle, (c) frequency deviation, (d) σ_{vm}, (e) σ_{pa}, and (f) σ_f.

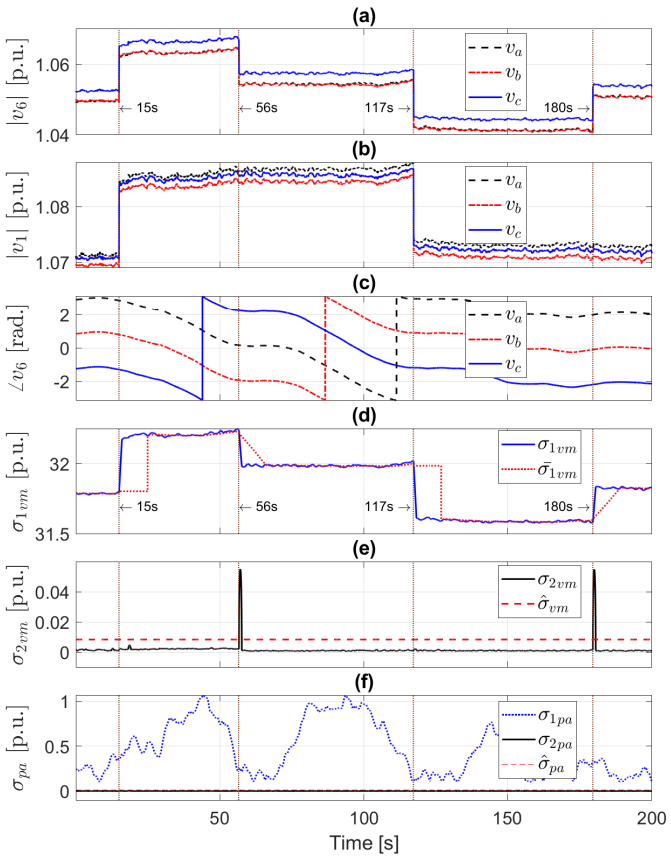

Fig. 6. Detection and classification of multiple voltage magnitude events caused by load switchings. (a) PMU-6 voltage magnitude, (b) PMU-1 voltage magnitude, (c) PMU-6 voltage phase angle, (d) σ_{1vm}, (e) σ_{2vm}, and (f) σ_{pa}.

short durations of a few cycles are usually caused by faults somewhere on the upstream power system. In order to achieve better resolution, Figure 5(c) depicts the deviation of frequency from its nominal value, i.e., $\Delta f = f - f_n$. Figures 5(d), (e), and (f) show that despite the small magnitudes of these events, the second singular value σ_{2i} of all system variables increases above the respective thresholds $\hat{\sigma}_i$. These events are detected and classified as faults by Line 2 of Algorithm 2.

Figures 6(a) and (b) show the 3-phase voltage magnitudes reported by PMU-6 and PMU-1, respectively. During a 200-second interval, four load switchings happen and cause step-like changes in voltage magnitude at around 15, 56, 117, and 180 seconds. However, two of these events (at around 56 and 180 seconds) are not spatially correlated since PMU-1 at the main substation has not reported them. Figure 6(d) shows the variations of the first singular value of voltage magnitude σ_{1vm} relative to its moving average value $\bar{\sigma}_{1vm}$. It can be seen that the two spatially correlated events (around 15s and 117s) cause a significant deviation of σ_{1vm} from its average value and trigger the detection flag $\bar{\phi}_{vm}$. However, the two spatially correlated events around 56s and 180s do not cause a deviation of more than $\alpha = 1\%$ from the average value, hence do not trigger $\bar{\phi}_{vm}$. Therefore, voltage events at 15s and 117s are classified as correlated events using Line 17 of Algorithm 2. It should be noted that as soon as $\bar{\phi}_{vm}$ is triggered, Algorithm 1 stops updating the moving average for L instants to prevent any false detections during the new settling point post-event.

On the other hand, the uncorrelated events at 56s and 180s cause a significant increase in the value of the second singular value σ_{2vm} of voltage magnitude matrix, as shown in Figure 6(e). Since σ_{2vm} increases above the threshold $\hat{\sigma}_{vm}$, Algorithm 1 declares an event and Line 4 of Algorithm 2 classifies it as an uncorrelated voltage event. Moreover, Figure 6(c) shows the three-phase voltage phase angle reported by PMU-6, and Figure 6(f) shows the first and second singular values of the phase angle matrix against the threshold $\hat{\sigma}pa$. As expected, the switching events do not trigger ϕ_{pa} or $\bar{\phi}_{pa}$.

Figures 7(a), (b), and (c) show the three-phase voltage magnitude and phase angle reported by PMU-5, and the frequencies measured by PMU-1, PMU-3, and PMU-5 during a 12s interval. As shown in Figure 7(b), a phase angle deviation happens at around 5.26s on “phase A" reported by PMU-5. This outlier does not significantly affect the singular values of voltage magnitude and frequency matrices shown in Figures 7(d) and (f). However, as shown in Figures 7(e), σ_{2pa} of the voltage phase angle matrix increases above the threshold $\hat{\sigma}_{pa}$ and triggers the detection flag ϕ_{pa}. Therefore, the event is classified as an uncorrelated phase angle event by Line 12 of Algorithm 2.

One major advantage of the proposed method is the reliability and robustness of the singular value thresholding criteria. In contrast to conventional SVD-based methods,

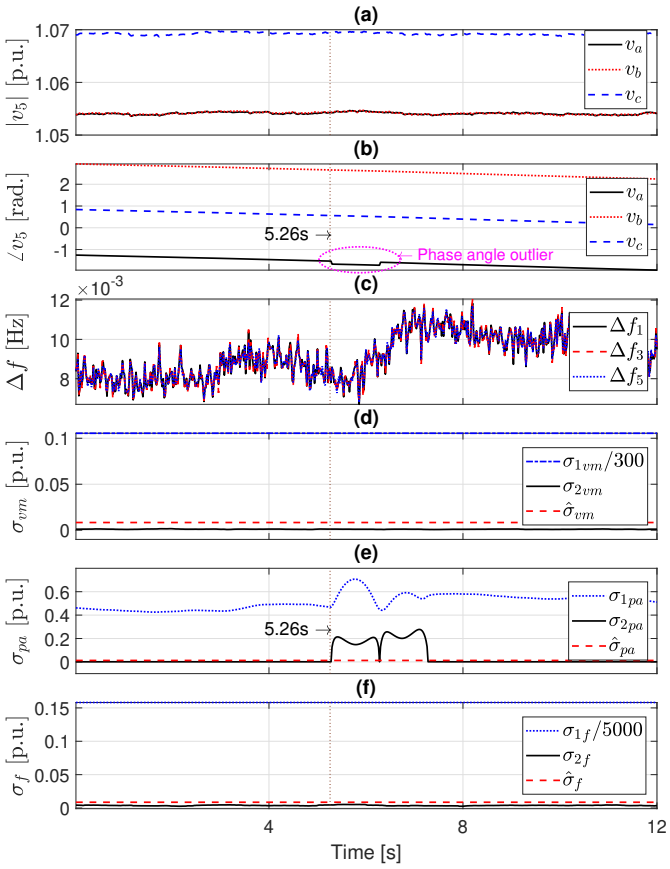

Fig. 7. Detection and classification of a voltage phase angle outlier. (a) PMU-5 voltage magnitude, (b) PMU-5 voltage phase angle, (c) frequency, (d) σ_{vm}, (e) σ_{pa}, and (f) σ_f.

the proposed method uses PMU accuracy information to determine dimensionality. Conventional SVD-based methods such as [10,11,14] use experimental threshold values to compare the largest singular values with the smaller ones and determine the dimensionality. In particular, [14] uses the following to approximate the rank ρ of $\mathbf{Y}$ as the largest r such that the following holds:

$$\begin{cases} \sigma_r/\sigma_{\bar{r}+1} > \Delta \\ (\sum_{r=1}^{\bar{r}} \sigma_r)/(\sum_{i=1}^{m} \sigma_i) \geq \tau \end{cases} \tag{13}$$

where Δ guarantees that only dominant singular values remain in the approximation and τ measures the approximation ratio of lower-dimension singular values to the magnitude of all singular values combined. In the current literature, these thresholds are defined experimentally and can cause under/over-estimation of the dimensionality, especially when the synchrophasor data is noisy and the spatiotemporal events have small magnitudes.

Figure 8 shows the comparison between dimensionality approximation performed by the proposed method and that of [14] with suggested $\Delta = 10$ and $\tau = 0.99$. Figures 8(a) and 8(b) show the voltage magnitudes and the estimated rank ρ by both methods. It can be seen that when it comes to events with small magnitude changes, only the proposed method can accurately detect the

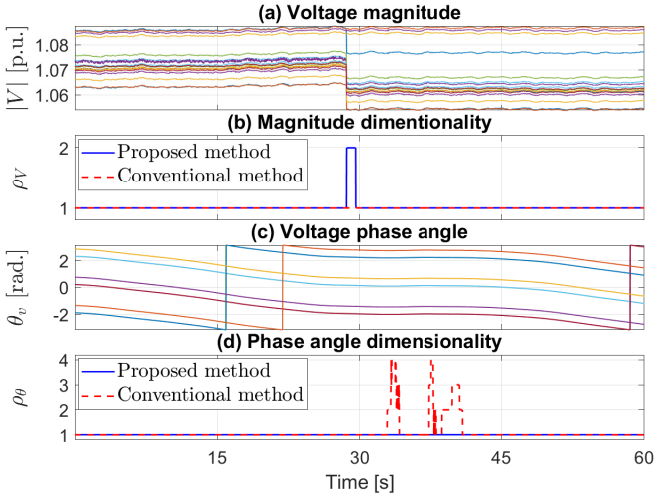

Fig. 8. Comparison of dimensionality approximation performed using the proposed method and a conventional SVD-based method.

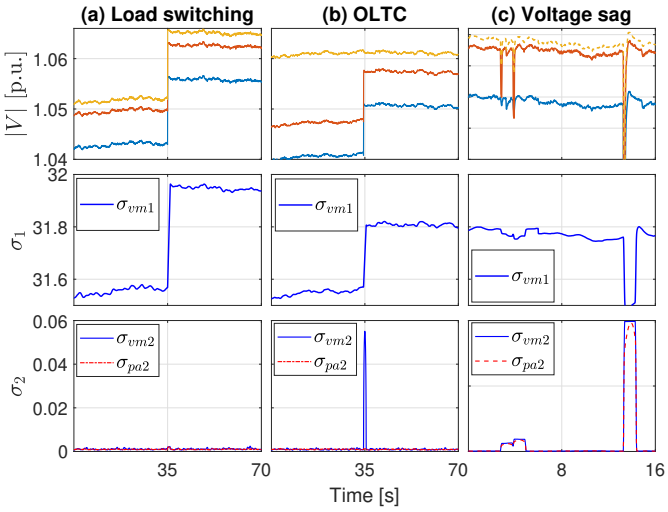

Fig. 9. Event classification: Impact on σ_1 and σ_2 due to (a) load switching, (b) OLTC operation, and (c) voltage sag events.

dimensionality change. On the other hand, in the case of phase angle, the higher-dimension singular values have larger magnitude compared to the lower-dimension ones, which can cause conventional thresholding methods to overestimate dimensionality. This has been shown in Figures 8(c) and 8(d). While phase angles, shown in Figures 8(c), are not experiencing any particular disturbance, the conventional thresholding method overestimates the rank due to the increase in the higher-dimension singular values caused by measurement accuracy. However, since the proposed method employs the phase angle error (AE) information of PMUs, the rank approximation is accurate and robust against such errors and noise.

Figure 9 shows the impact on σ_1 and σ_2 due to different events and confirms the classification Algorithm 2. Figure 9(a) shows the results for load switching where $\bar{\phi}_{vm}$ is triggered and while there are no significant deviations in σ_{vm2} and σ_{pa2}, the first singular value σ_{vm1} shows the most deviation. This confirms Line 17 of Algorithm 2. Figure 9(b) and Figure 9(c)

TABLE II
RUNTIME OF THE PROPOSED METHOD FOR DIFFERENT NUMBERS OF PMUS

No. PMUs (n)	Runtime [ms] Average	Maximum
6	0.164	2.097
50	1.535	3.861
100	1.895	4.394
1000	6.803	15.10

depict uncorrelated OLTC operation and voltage sag events, respectively, where ϕ_{vm} is triggered. However, σ_{pa2} only deviates in the case of voltage sag event, confirming Lines 6 and 9 of Algorithm 2.

The main computational burden of the proposed method is the computation of the SVD performed three times at each instant. While the runtime of the classification algorithm flags is relatively constant, the runtime of the detection algorithm highly depends on the number of PMUs impacting the computational burden of SVD. Table II shows the average and maximum runtime of the proposed method at each instant calculated with different number of PMUs and synthetic data. Even with $n = 1000$, the detection and classification procedure terminates within the $1/F_s = 20$ ms window and before the next data messages arrive. In addition to the algorithm runtime, the total event detection delay depends on PMU communication delay, PDC wait time (usually under 100ms), and $1/F_s$ resulting from the moving window updates.

VI. CONCLUSIONS

This paper proposes an SVD-based event detection and classification method. The SVD-based detection algorithm evaluates the dimensionality of real-time sliding matrices containing the voltage magnitude, phase angle, and frequency data reported by PMUs across the power system. The proposed detection flags are set according to the changes in the dimensionality of matrices that indicate disruption of the low-rank nature of synchrophasor data by an event. The classification algorithm comprises a physics-based decision tree that employs the detection flags and first and second singular values. Spatially correlated and uncorrelated events are classified under several categories, i.e., faults, voltage sag, load switching, OLTC operation, voltage phase angle impulse, islanding, frequency oscillations and generation-load mismatch. The performance of the proposed method is evaluated using field PMU data containing different types of events and outliers. The numerical results show that the proposed detection and classification method is accurate and reliable even in the presence of PMU data uncertainty.

VII. ACKNOWLEDGMENT

The authors are grateful to Professor Mario Paolone for his insight, and for providing the EPFL campus smart grid information and PMU data.

REFERENCES

[1] "IEEE standard for synchrophasor measurements for power systems," *IEEE Std C37.118.1-2011 (Revision of IEEE Std C37.118-2005)*, pp. 1–61, 2011.

[2] D. R. Gurusinghe and A. D. Rajapakse, "Post-disturbance transient stability status prediction using synchrophasor measurements," *IEEE Trans. Power Syst.*, vol. 31, no. 5, pp. 3656–3664, 2016.

[3] T. Wu, Y. J. Zhang, and X. Tang, "Online detection of events with low-quality synchrophasor measurements based on iforest," *IEEE Trans. Ind. Informat.*, pp. 1–1, 2020.

[4] M. Cui, J. Wang *et al.*, "A novel event detection method using PMU data with high precision," *IEEE Trans. Power Syst.*, vol. 34, no. 1, pp. 454–466, 2019, detection.

[5] S. S. Negi, N. Kishor, K. Uhlen, and R. Negi, "Event detection and its signal characterization in PMU data stream," *IEEE Trans. Ind. Informat.*, vol. 13, no. 6, pp. 3108–3118, 2017, detection.

[6] S. Pandey, A. Srivastava, and B. Amidan, "A real time event detection, classification and localization using synchrophasor data," *IEEE Trans. Power Syst.*, pp. 1–1, 2020, detection.

[7] A. Vosughi, K. S. Sajan, and A. Srivastava, "Synchrophasor-based event detection, classification and localization using koopman, transient energy matrix, best worth method, and dynamic graph," *IEEE Transactions on Power Delivery*, pp. 1–1, 2021, detection.

[8] R. Pourramezan, H. Karimi, J. Mahseredjian, and M. Paolone, "Real-time processing and quality improvement of synchrophasor data," *IEEE Trans. Smart Grid*, vol. 11, no. 4, pp. 3313–3324, 2020.

[9] R. Pourramezan, R. Hassani, H. Karimi, M. Paolone, and J. Mahseredjian, "A real-time synchrophasor data compression method using singular value decomposition," *IEEE Transactions on Smart Grid*, vol. 13, no. 1, pp. 564–575, 2022.

[10] P. H. Gadde, M. Biswal *et al.*, "Efficient compression of PMU data in WAMS," *IEEE Trans. Smart Grid*, vol. 7, no. 5, pp. 2406–2413, 2016.

[11] W. Wang, C. Chen *et al.*, "Synchrophasor data compression under disturbance conditions via cross-entropy-based singular value decomposition," *IEEE Trans. Ind. Informat.*, pp. 1–1, 2020.

[12] K. Mahapatra, N. R. Chaudhuri *et al.*, "Online analytical characterization of outliers in synchrophasor measurements: A singular value perturbation viewpoint," *IEEE Trans. Power Syst.*, vol. PP, no. 99, pp. 1–1, 2017.

[13] L. Xie, Y. Chen, and P. R. Kumar, "Dimensionality reduction of synchrophasor data for early event detection: Linearized analysis," *IEEE Transactions on Power Systems*, vol. 29, no. 6, pp. 2784–2794, 2014.

[14] W. Li, M. Wang, and J. H. Chow, "Real-time event identification through low-dimensional subspace characterization of high-dimensional synchrophasor data," *IEEE Transactions on Power Systems*, vol. 33, no. 5, pp. 4937–4947, 2018.

[15] P. Gao, M. Wang *et al.*, "Missing data recovery by exploiting low-dimensionality in power system synchrophasor measurements," *IEEE Trans. Power Syst.*, vol. 31, no. 2, pp. 1006–1013, 2016.

[16] R. Pourramezan, H. Karimi, and J. Mahseredjian, "Real-time disturbance detection and classification using principal component analysis of PMU data," in *2020 IEEE Power & Energy Society General Meeting (PESGM)*, Conference Proceedings, pp. 1–5, detection.

[17] A. Derviškadić, P. Romano *et al.*, "Architecture and experimental validation of a low-latency phasor data concentrator," *IEEE Trans. Smart Grid*, vol. 9, no. 4, pp. 2885–2893, 2018.

[18] B. P. Epps and E. M. Krivitzky, "Singular value decomposition of noisy data: mode corruption," *Experiments in Fluids*, vol. 60, no. 8, pp. 1–30, 2019.

[19] B. P. Epps and A. H. Techet, "An error threshold criterion for singular value decomposition modes extracted from PIV data," *Experiments in Fluids*, vol. 48, no. 2, pp. 355–367, 2010.

[20] C. Eckart and G. Young, "The approximation of one matrix by another of lower rank," *Psychometrika*, vol. 1, no. 3, pp. 211–218, 1936.

[21] P. Romano and M. Paolone, "Enhanced interpolated-DFT for synchrophasor estimation in FPGAs: Theory, implementation, and validation of a PMU prototype," *IEEE Trans. Instrum. Meas*, vol. 63, no. 12, pp. 2824–2836, 2014.

[22] M. Pignati, M. Popovic *et al.*, "Real-time state estimation of the EPFL-Campus medium-voltage grid by using PMUs," in *IEEE PES ISGT 2015*, 2015, pp. 1–5.

[23] G. Frigo, A. Derviškadić, Y. Zuo, A. Bach, and M. Paolone, "Taylor-Fourier PMU on a real-time simulator: Design, implementation and characterization," in *2019 IEEE Milan PowerTech*, 2019, pp. 1–6.